Letters

High-Frequency Oscillation Mechanism Analysis and Suppression Method of VSC-HVDC

Jianhang Zhu, *Student Member, IEEE*, Jiabing Hu, *Senior Member, IEEE*, Lei Lin, *Member, IEEE*, Yifan Wang, and Chao Wei

***Abstract*—This letter studies the high-frequency oscillation (HFO) of voltage-source converters (VSCs) in high-voltage dc transmission (HVDC). The oscillation mechanism shows that a long-time delay of the control system is the main factor affecting HFO. The existing HFO suppression schemes by software optimization, such as adding a low-pass filter (LPF) to the terminal voltage feedforward control (TVFC), etc., do not eliminate the risk of HFO. Thus, based on the mechanism analysis via the Nyquist curves in the complex plane, the design principles of the improved suppression method are proposed. Finally, the proposed schemes were confirmed by the experimental results.**

***Index Terms*—Delay loop, high-frequency oscillation (HFO), suppression method, voltage-source converters (VSCs).**

I. Introduction

With the rapid development of power electronics, a large number of voltage-source converters (VSCs) have been applied to modern power systems. After several reports of high-frequency oscillation (HFO) instability issues [1]–[3] in different fields, the corresponding analyses and suppressions have become an important research topic.

Based on the HFO instability analysis in [3], the outer loop and phase looked-loop (PLL) controller make few contributions to HFO due to the low bandwidth designs. Thus, the small-signal model suitable for HFO only needs to consider the current controller. To suppress the HFO of VSC, some schemes have been proposed through the optimization of hardware and software, respectively. For the former method, the investment will be increased. Besides, when the structure of the power network is changed, the suppression effect may be significantly reduced. Then, some additional controllers have been proposed by passivity-based controller design [4]. However, the results from case by case do not consider the effect on the entire high-frequency range (HFR). In most cases, these just reduce the risk of HFO instability.

Manuscript received December 26, 2019; revised January 28, 2020; accepted February 11, 2020. Date of publication February 19, 2020; date of current version May 1, 2020. This work was supported by the National Key Research and Development Program under Grant 2016YFB0900100. *(Corresponding author: Jiabing Hu.)*

The authors are with the State Key Laboratory of Advanced Electromagnetic Engineering and Technology, and School of Electrical and Electronic Engineering, Huazhong University of Science and Technology, Wuhan 430074, China (e-mail: jh_zhu@hust.edu.cn; j.hu@mail.hust.edu.cn; linlei@hust.edu.cn; yifan_wang@hust.edu.cn; weic@hust.edu.cn).

Color versions of one or more of the figures in this letter are available online at http://ieeexplore.ieee.org.

Digital Object Identifier 10.1109/TPEL.2020.2975092

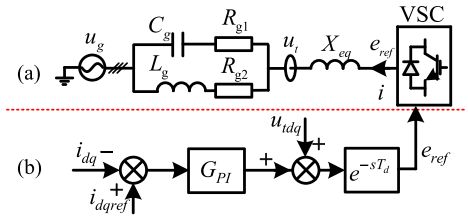

Fig. 1. Grid-connected VSC-HVDC for HFO analysis.

Compared with the small capacity grid-connected VSCs, the VSC-HVDCs, such as modular multilevel converters (MMCs), have other different features. First of all, the multiple control algorithms and lots of signal transmission result in a significant increase in controller delay [2]. Next in importance, the internal dynamics are negligible [5], [6]. Finally, the ac filter is removed due to the lower distortions of ac outputs. Therefore, in order to suppress the HFO of VSC-HVDC, the mechanism analyses with these new features are given first in Section II. For the different influencing factors, the design principles of the suppression method are proposed in Section III. Then, Section IV gives the experimental results of the proposed schemes. Finally, the conclusion is drawn in Section V.

II. Mechanism Analysis of VSC-HVDC

The grid-connected VSC-HVDC system for HFO analysis is shown in Fig. 1(a), where i is the ac current, $e_{\rm ref}$ is the internal voltage of VSC, which connects with the point of common coupling through an equivalent inductance and resistance $X_{\rm eq}$ (i.e., $L_{\rm eq} + R_{\rm eq}$). The total control time delay is simulated by T_d. The ac network is composed of passive components C_g, L_g, R_{g1}, and R_{g2}. The control system ignores the effect of the outer loop and PLL controls, and the current control is shown in Fig. 1(b), which only contains proportional–integral (PI) control and terminal voltage feedforward control (TVFC). These parameters are based on the Luxi VSC-HVDC project in [2].

At this time, the state equation of the closed-loop system in the synchronously rotating reference frame can be established easily, and it is no longer given here due to the space limit. The delay loop is approximated by the Pade function.

TABLE I
MAXIMUM VALUE OF REAL PART OF EIGENVALUES

Pade order	Max real part	Pade order	Max real part
1	-5.130	5	491.6
2	211.6	6	490.7
3	530.1	7	490.7
4	500.0	8	490.7

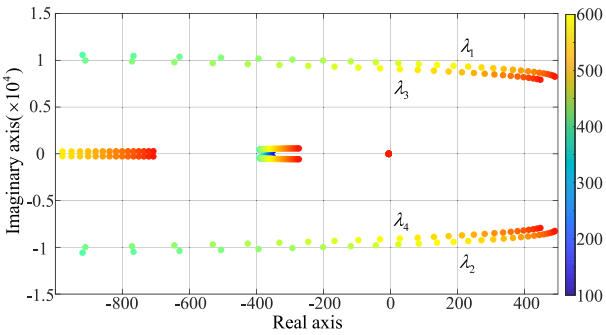

Fig. 2. Eigenvalue locus of the closed-loop system with time-delay varying from 100 to 600 μs.

When the time delay is 600 μs, the maximum value of the real part of eigenvalues for different Pade order n_{de} is shown in Table I, and the n_{de} should be set to 6 for accurate analysis of a long delay system. When the time delay varies from 100 to 600 μs, the eigenvalues locus of the closed-loop system is shown in Fig. 2, and two pairs of eigenvalues, $\lambda_{1,2}$ and $\lambda_{3,4}$, cross the imaginary axis and reach the right half-plane of the complex plane with high modal frequency, so time delay is the important cause for the HFO issue.

Since the network is composed of passive components (i.e., inductors, resistors, and capacitors), its frequency characteristic may vary between capacitive and inductive irregular (i.e., the phase varies between $\pm 90°$). Based on the Nyquist stability criterion [7], when the phase of VSC-HVDC's frequency characteristic exceeds $\pm 90°$, the grid-connected system will have the risk of unstable.

The transfer function from i to u_t in the DQ reference frame can be expressed as

$$u_t = -\left(L_{\mathrm{eq}}s + R_{\mathrm{eq}} + G_{\mathrm{PI}}e^{-sT_d}\right)/\left(1 - e^{-sT_d}\right) i = -G_{\mathrm{iu}} i \tag{1}$$

where $G_{\mathrm{PI}} = k_p + k_i/\mathrm{s}$.

As shown in Fig. 3(a), the phase of G_{iu} in HFR exceeds $+90°$, and with the increase of time delay, the risk region will increase. Besides, although G_{iu} can be used for HFO analysis, it may not be friendly for the mechanism analysis. Based on the concept of motion equation [8], the internal voltage is the interface to reflect the system behavior of VSC. So, G_{iu} is transformed as

$$u_t = -G_{\mathrm{iu}} i = -\left(G_{\mathrm{ie}} + \left(L_{\mathrm{eq}}s + R_{\mathrm{eq}}\right)\right) i \tag{2}$$

where

$$G_{\mathrm{ie}} = \underbrace{\left(L_{\mathrm{eq}}s + R_{\mathrm{eq}} + G_{\mathrm{PI}}\right)}_{G_{\mathrm{ie1}}} \underbrace{e^{-sT_d}/\left(1 - e^{-sT_d}\right)}_{G_{\mathrm{ie2}}}. \tag{3}$$

The Bode diagrams for each part of (3) are shown in Fig. 3(c). The time delay loop in G_{ie2} causes the phase jump between $\pm 180°$ in HFR, which is the essential reason for the risk of HFO.

One of the existing HFO suppression schemes by controller optimization is adding a low-pass filter (LPF) to TVFC [2] given as follows:

$$G_{\mathrm{lpf}} = \alpha_f/(s + \alpha_f) \tag{4}$$

where α_f is the bandwidth of LPF G_{lpf}.

The optimized results of G_{ie1} and G_{ie2} are shown in Fig. 3(d). The phase of G_{ie1} and the magnitude of G_{ie2} are changed obviously. Compared to the results of Fig. 3(c) and (d), the LPF mainly reduces the magnitude of G_{ie} in HFR, and the phase of G_{ie} also varies between $\pm 180°$. When we observe the frequency characteristic of VSC by G_{iu}, as shown in Fig. 3(b), the resonance peak of the magnitude of G_{iu} is eliminated by the LPF, and the phase angle is limited between $0°$ and $+90°$ for most frequency ranges. So the LPF has a certain function of suppressing HFO in some cases. Based on the abovementioned analysis, we can find that the underlying mechanism of this filter is to reduce the amplitude of G_{ie} in HFR. These can be explained more intuitively by the Nyquist curves in the complex plane, and a positive real part (i.e., the first and fourth quadrants) indicates positive damping. As shown in Fig. 3(e) and (f), G_{ie} is limited to a small ring by the LPF. Combining the effect of equivalent reactance (i.e., $L_{\mathrm{eq}}s + R_{\mathrm{eq}}$), G_{iu} locus in the first and second quadrants. So this suppression scheme cannot eliminate the risk of HFO. Besides, a larger equivalent reactance (i.e., R_{eq}) will be of benefit for HFO suppression. For an HVDC project, the feedforward voltage u_t can be set on the high-voltage side of the transformer, and the leakage reactance will be helpful to reduce the risk of HFO.

III. PROPOSED SUPPRESSION SOLUTION FOR HFO

According to the abovementioned mechanism analysis, an ideal HFO suppression method is to transform G_{ie} to the right half-plane of the complex plane without affecting the normal operation. However, it is difficult to achieve only with controller optimization. So our design principle of suppressing HFO is to reduce the amplitude of G_{ie} in HFR to zero. Then, combining the effect of equivalent resistance R_{eq}, the risk of HFO will be eliminated.

Initially, the amplitude of G_{ie} is dominated by $(L_{\mathrm{eq}}s + R_{\mathrm{eq}})$, and its integral operation causes the amplitude of G_{ie} to increase with frequency. So, as shown in Fig. 4, an LPF (i.e., G^u_{lpf}) is introduced into the TVFC path. With the bandwidth decreases of the filter, the amplitude of $(L_{\mathrm{eq}}s + R_{\mathrm{eq}})$ is reduced effectively in Fig. 5(a). However, a lower bandwidth will affect the dynamic performance of the system. Besides, the amplitude of $(L_{\mathrm{eq}}s + R_{\mathrm{eq}})$ can be reduced further by increasing the order of G^u_{lpf}, which is achieved by cascading the first-order LPF. The effects of the G^u_{lpf}'s order on $(L_{\mathrm{eq}}s + R_{\mathrm{eq}})$ with 100 Hz bandwidth are shown in Fig. 5(b). Although the amplitude of $(L_{\mathrm{eq}}s + R_{\mathrm{eq}})$ gets further smaller, the real part of Nyquist curves (i.e., the

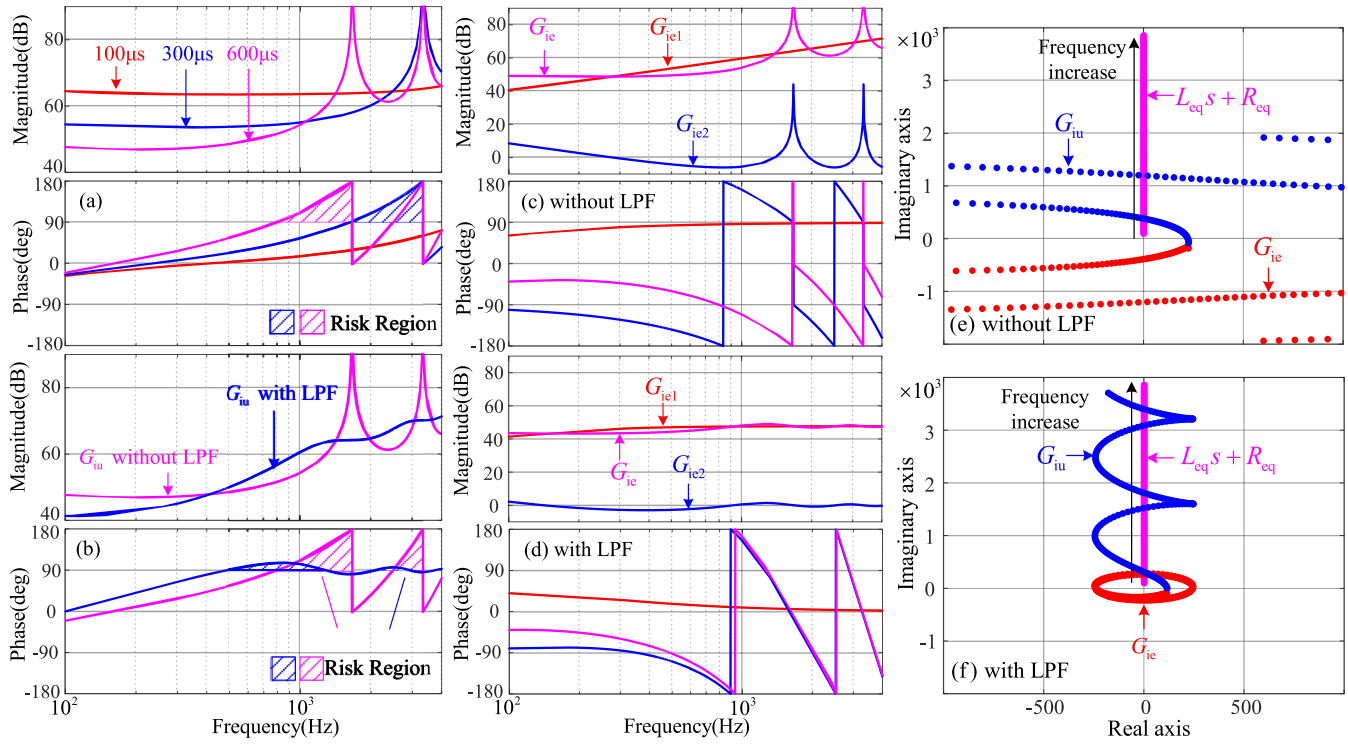

Fig. 3. (a) Effect of time delay on the transfer function $G_{\rm iu}$. (b) Bode diagram of $G_{\rm iu}$ with and without LPF $G_{\rm lpf}$. (c) Bode diagram of $G_{\rm ie1}$, $G_{\rm ie2}$, and $G_{\rm ie}$ without LPF $G_{\rm lpf}$. (d) Bode diagram of $G_{\rm ie1}$, $G_{\rm ie2}$, and $G_{\rm ie}$ with LPF $G_{\rm lpf}$. (e) Nyquist curves of $G_{\rm ie}$, $L_{\rm eq}s+R_{\rm eq}$, and $G_{\rm iu}$ without LPF $G_{\rm lpf}$. (f) Nyquist curves of $G_{\rm ie}$, $L_{\rm eq}s+R_{\rm eq}$, and $G_{\rm iu}$ with LPF $G_{\rm lpf}$.

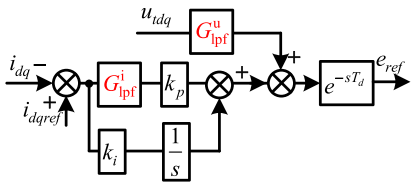

Fig. 4. Proposed suppression solution in the current control system.

TABLE II
FREQUENCY RANGE OF HFO SUPPRESSION UNDER DIFFERENT ORDER OF LPFS

Order (G^{u}_{lpf}/G^{i}_{lpf})	Frequency range (Hz)	Order (G^{u}_{lpf}/G^{i}_{lpf})	Frequency range (Hz)	Order (G^{u}_{lpf}/G^{i}_{lpf})	Frequency range (Hz)
1/0	/	1/1	/	1/2	/
2/0	/	2/1	>1147	2/2	>685
3/0	/	3/1	>1133	3/2	>651
4/0	/	4/1	>1135	4/2	>648

where '/' indicates that the risk of high-frequency oscillations still exists.

total damping) of $G_{\rm iu}$ in Fig. 5(c) still varies between positive and negative.

As shown in Fig. 5(b), The transfer function $G_{\rm PI}$ mainly affects the amplitude of $G_{\rm ie}$ at this time, which can be divided into two parts (i.e., k_p and k_i/s). The main influence factor is k_p, and a smaller k_p can reduce the region of negative damping, but this may affect the performance of the normal operation. Therefore, an LPF (i.e., $G^{i}_{\rm lpf}$) is introduced into the k_p path in Fig. 4. When $G^{u}_{\rm lpf}$ is set to a third-order LPF with 100 Hz bandwidth, the effects of the bandwidth and the order of $G^{i}_{\rm lpf}$ on the real part of Nyquist curves of $G_{\rm iu}$ are shown in Fig. 6(d) and (e), respectively. Similar to the law of $G^{u}_{\rm lpf}$, a lower bandwidth and a higher order will be beneficial to the suppression of HFO.

The comprehensive optimization results of a third-order $G^{u}_{\rm lpf}$ with 100 Hz bandwidth and a second-order $G^{i}_{\rm lpf}$ with 200 Hz bandwidth are shown in Fig. 6(c). The risk of HFO for the frequency above 553 Hz is eliminated effectively. Besides, if the oscillation frequency is not so high, the small-signal model needs to be re-established, and other influencing factors, such as the internal dynamics in MMC-HVDC, should be considered. These will be studied in the future.

IV. EXPERIMENTAL VERIFICATION

As shown in Fig. 7, a three-phase MMC prototype is built to verify the proposed suppression method, and the power network is simulated by the passive components *RLC*. The control system only contains the ac current and PLL controller. The carrier frequency of the phase-disposition pulsewidth modulation (PD-PWM) is 5 kHz, so the equivalent switching frequency is far away from the oscillation frequency.

At this time, the influence of orders of $G^{u}_{\rm lpf}$ (100 Hz bandwidth) and $G^{i}_{\rm lpf}$ (300 Hz bandwidth) on the frequency range of HFO suppression is shown in Table II, where the total delay is about 380 μs after adding time delay 200 μs, $k_p=14$, $k_i=2000$, and $R_{\rm eq}\approx 2.4\ \Omega$. The appropriate orders can be selected according to the oscillation frequency of HFO. Besides, the effect of the bandwidth of LPFs will be studied in the future.

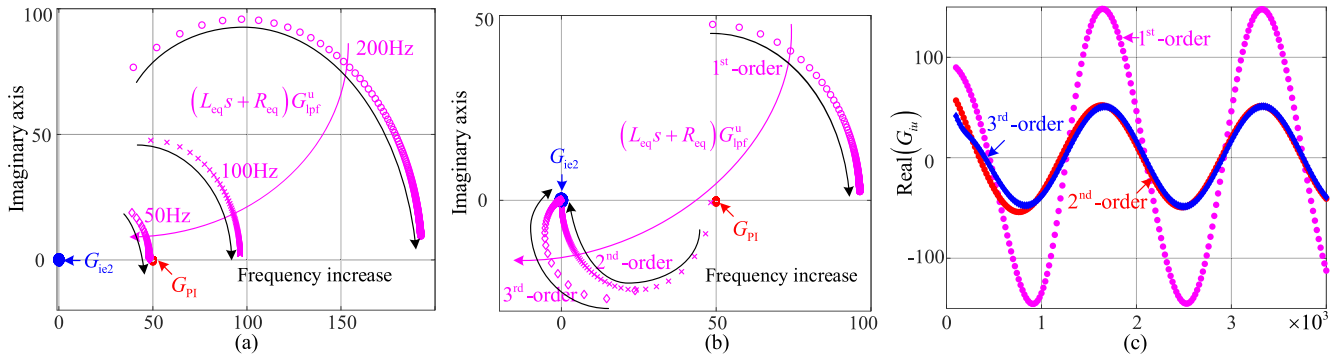

Fig. 5. (a) Nyquist curves of each part of $G_{\rm ie}$ with the bandwidth of first-order LPF $G^u_{\rm lpf}$ varying from 50 to 200 Hz. (b) Nyquist curves of each part of $G_{\rm ie}$ with the order of 100 Hz bandwidth LPF $G^u_{\rm lpf}$ varying from 1 to 3. (c) Real part of Nyquist curves of $G_{\rm iu}$ with the order of 100 Hz bandwidth LPF $G^u_{\rm lpf}$ varying from 1 to 3.

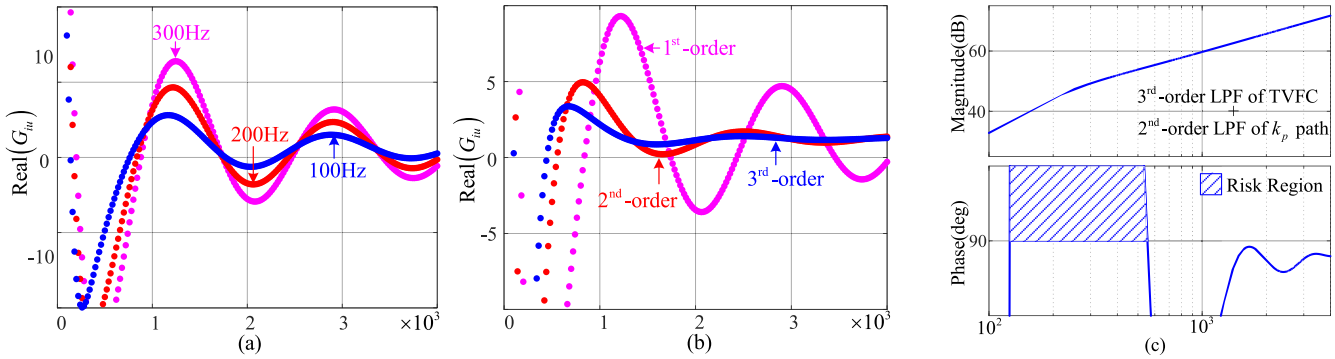

Fig. 6. (a) Real part of Nyquist curves of $G_{\rm iu}$ with the bandwidth of first-order LPF $G^i_{\rm lpf}$ varying from 100 to 300 Hz. (b) Real part of Nyquist curves of $G_{\rm iu}$ with the order of 200 Hz bandwidth LPF $G^i_{\rm lpf}$ varying from 1 to 3. (c) Bode diagram of $G_{\rm iu}$ with the comprehensive suppression method.

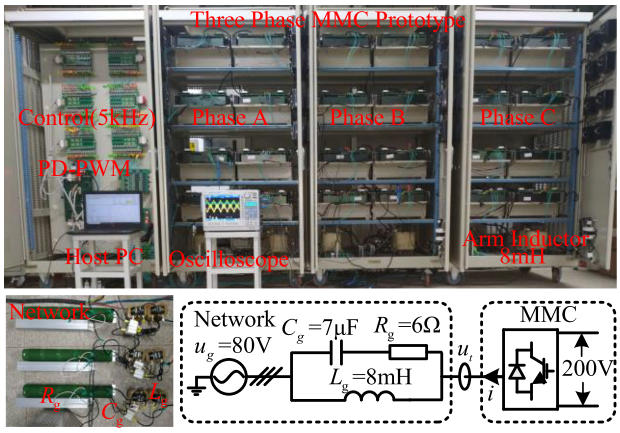

Fig. 7. Prototype of a grid-connected MMC system.

In order to verify the analysis mentioned above, three cases are designed for experiments, and their difference is the parameters of the ac network. The first case verifies the effects of LPF-TVFC in suppressing HFO, which has been studied initially in [2]. The corresponding network parameters have been marked in Fig. 7. After adding an additional time delay 200 μs to the control system, the ac current will oscillate at about 1223 Hz in Fig. 8(a.1). Then, implementing the suppressing scheme of adding a first-order LPF with 100 Hz bandwidth to TVFC, the HFO is suppressed in Fig. 8(b.1). However, the risk of HFO still exists, and it will be illustrated in case 2, which changes the grid parameters to $R_g = 4.5\ \Omega$, $L_g = 8$ mH, $C_g = 7\ \mu$F. As shown in Fig. 8(a.2), the method in case 1 cannot suppress the HFO effectively. Then, without changing the bandwidth of TVFC-LPF, only increasing its order to three, the result in Fig. 8(b.2) shows that this suppressing method is valid. Based on the mechanism analysis mentioned above, the contribution of TVFC to the risk of HFO is small at this time, and the main factor is the k_p path of the current control. So the instability of HFO can also be designed, and the grid parameters are modified to $R_g = 4.2\ \Omega$, $L_g = 8$ mH, $C_g = 9\ \mu$F in case 3. As shown in Fig. 8(a.3), the HFO suppressing method in case 2 failed at this time. Therefore, we further added a first-order LPF with 300 Hz bandwidth to the path k_p of current control, and the result in Fig. 8(b.3) shows that the HFO disappears completely. Therefore, the effectiveness of the proposed design principles of the HFO suppression scheme is verified. Meanwhile, the results in Fig. 8(c.1)–(c.3) show that the submodule capacitor voltages of upper and lower bridge arm do not change significantly when HFO occurs and some suppression measures are implemented, so the proposed LPFs do not influence the internal operation characteristics of MMC.

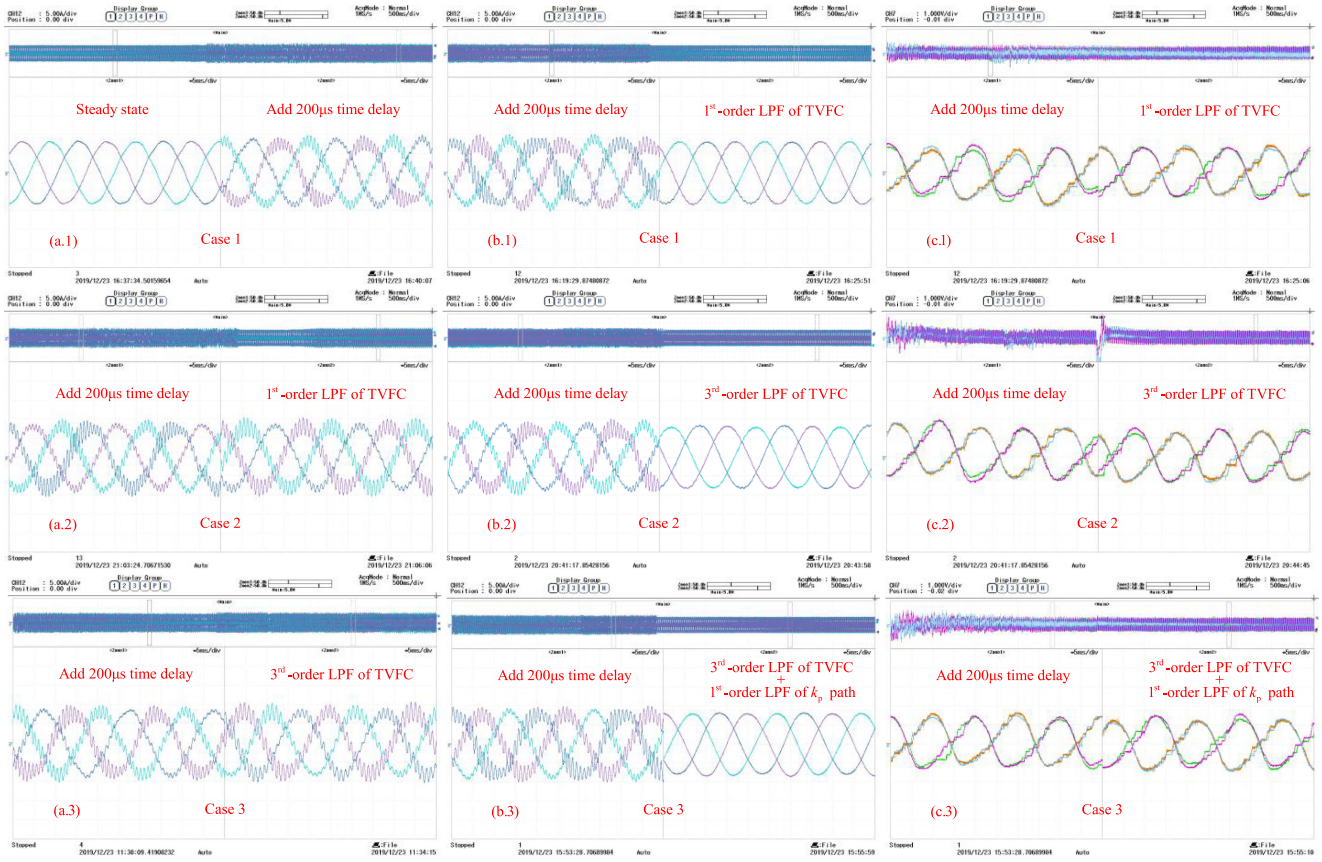

Fig. 8. Experimental results of (a) and (b) ac currents and (c) submodule capacitor voltage for three cases. Case 1 (a) Adding 200 μs time delay to the control system. (b) and (c) Adding a first-order LPF to TVFC. Case 2 (a) Adding a first-order LPF TVFC. (b) and (c) Adding a third-order LPF to TVFC. Case 3 (a) Adding a third-order LPF to TVFC. (b) and (c) Adding a third-order LPF to TVFC and a first-order LPF to the path k_p of current control.

V. Conclusion

In this letter, the underlying mechanism analysis of VSCs-HFO is given first. The phase jump caused by the controller's time delay is the leading factor causing instability of HFO. Based on the Nyquist curves in the complex plane, the effects of each part of the transfer function between internal voltage and ac current are analyzed. Besides, a larger equivalent reactance of ac output will be helpful for HFO suppression. Then, based on the principle of reducing the amplitude characteristic in HFR, some detailed suppressing schemes are proposed, and the combined effects of the TVFC-LPF and the LPF in the proportional path of current control have an excellent suppression effect on HFO, which have been verified by experiments.

References

[1] C. Buchhagen, C. Rauscher, A. Menze, and J. Jung, "BorWin1—First experiences with harmonic interactions in converter dominated grids," in *Proc. Int. ETG Congr. Die Energiewende - Blueprints New Energy Age*, 2015, pp. 1–7.

[2] C. Zou *et al.*, "Analysis of resonance between a VSC-HVDC converter and the AC grid," *IEEE Trans. Power Electron.*, vol. 33, no. 12, pp. 10157–10168, Dec. 2018.

[3] H. Tao, H. Hu, X. Zhu, Y. Zhou, and Z. He, "Harmonic instability analysis and suppression method based on $\alpha\beta$- frame impedance for trains and network interaction system," *IEEE Trans. Energy Convers.*, vol. 34, no. 2, pp. 1124–1134, Jun. 2019.

[4] L. Harnefors, A. G. Yepes, A. Vidal, and J. Doval-Gandoy, "Passivity-based controller design of grid-connected VSCs for prevention of electrical resonance instability," *IEEE Trans. Ind. Electron.*, vol. 62, no. 2, pp. 702–710, Feb. 2015.

[5] J. Sun and H. C. Liu, "Sequence impedance modeling of modular multilevel converters," *IEEE J. Emerg. Sel. Topics Power Electron.*, vol. 5, no. 4, pp. 1427–1443, Dec. 2017.

[6] H. Wu, X. Wang, L. Kocewiak, and L. Harnefors, "AC impedance modeling of modular multilevel converters and two-level voltage-source converters: Similarities and differences," in *Proc. IEEE 19th Workshop Control Model. Power Electron.*, 2018, pp. 1–8.

[7] R. D. Middlebrook, "Input filter considerations in design and application of switching regulators," in *Proc. IEEE Ind. Appl. Soc. Annu. Meeting*, 1976, pp. 366–382.

[8] H. Yuan, X. Yuan, and J. Hu, "Modeling of grid-connected VSCs for power system small-signal stability analysis in DC-link voltage control timescale," *IEEE Trans. Power Syst.*, vol. 31, no. 5, pp. 3981–3991, Sep. 2017.